Characterization of the ZrCo–Hydrogen System in View of Its Use for Tritium Storage

M. Devillers, M. Sirch, S. Bredendiek-Kämper, and R.-D. Penzhorn*

Kernforschungszentrum Karlsruhe, Institut für Radiochemie, Postfach 36 40, D-7500 Karlsruhe, West Germany

Received September 6, 1989

To evaluate ZrCo as a getter material for the storage of tritium, a study on as-received and activated ZrCo as well as on $ZrCoH_x$ was carried out employing surface analytical methods such as XPS, AES, and electron microprobe. Complementary information on the bulk of the various species was obtained from X-ray diffraction. Loading ZrCo with hydrogen ($0.4 < p_{H_2} < 17.5$ MPa) at room temperature yielded $ZrCoH_x$ with $x = 2.91 \pm 0.04$. Pressure–composition loading and deloading isotherms for the systems $ZrCo/H_2$ and $ZrCo/D_2$ were determinated at temperatures below 300 °C. The hysteresis factor was quantified. The average enthalpy change and entropy change for the absorption of hydrogen (or deuterium) were found to be -81.5 ± 1.6 kJ/mol (-87.5 ± 0.8 kJ/mol) and -132.7 ± 2.7 J/mol·K (-146.4 ± 2.3 J/mol·K) respectively for the plateau region ($0.8 < x < 2.0$). Temperature cycling under isopleth conditions caused a small trapping that is restricted to the plateau region.

Introduction

Intermetallic compounds that absorb large quantities of hydrogen gas are of technological interest to tritium-processing facilities, provided the hydrogen is rapidly absorbed, the immobilized gas can be easily recovered, and the hydride is reasonably stable toward air and other gaseous impurities of the fusion fuel cycle. One promising intermetallic compound that could substitute uranium for the transport, storage, and pumping of tritium is ZrCo.[1-3] ZrCo alloy with a 1:1 ratio of the component atoms was selected after Padurets et al.[4] showed in very careful work with various ZrCo alloys that an intermetallic compound of this composition absorbs the largest amount of hydrogen.

In this article we report on measurements on the absorption and desorption isotherms of hydrogen and deuterium in ZrCo using a volumetric technique. The employed ZrCo alloy samples were characterized by several surface analytical methods. In view of its practical importance, particular attention was also paid to the hysteresis effect and the hydrogen trapping that occurs during isopleth temperature cycling.

Experimental Section

1. Reagents. Ingots of ZrCo alloy (60.8 wt % Zr and 39.2 wt % Co) supplied by SAES Getters (Milano, Italy) were employed in most experiments. The ingots were obtained from arc melting of a high-purity Zr sponge (Hf < 0.01 wt %) and Co blocks (Fe = 0.06 and Ni = 0.001 wt %) at 1450 °C under a vacuum of 10^{-2} Pa in a graphite crucible. Solidification of the molten alloy occurred in a water-cooled SS mould. Carbon contamination was found to be of the order of 900 ppm. Metallographic analysis performed on cross sections of the alloy confirmed the presence of a monophasic structure consisting of crystals of the ZrCo intermetallic compound.[5]

In a few runs a ZrCo powder sample kindly supplied by S. Konishi (JAERI, Tokaimura, Japan) was used.

Hydrogen (purity 99.9999%) was supplied by Messer-Griesheim (Krefeld, FRG) and used without further purification. Deuterium (purity in deuterium 99.8%) was obtained from Air Liquide (Düsseldorf-Holthausen, FRG) and purified by permeation through a palladium/silver membrane manufactured by Heraeus (Hanau, FRG) and operated at 400 °C.

2. Apparatus. High pressure ($p < 2 \times 10^7$ Pa) experiments with hydrogen at temperatures up to 200 °C were carried out in a 0.5-L SS autoclave manufactured by Haage (Mülheim/Ruhr, FRG).

The ultrahigh vacuum apparatus used for the absorption/desorption runs employing gases at pressures up to 130 kPa, shown schematically in Figure 1, is a modified version of the equipment described in a previous publication.[1] Loading data were generally obtained by the addition of successive amounts of hydrogen to the reactant powder kept at constant temperature. After the attainment of equilibrium, the gas uptake was determined volumetrically from the pressure decrease in one of several calibrated volumes with a MKS-Baratron Type 170 M-6C capacitance manometer. Isothermal deloading data were obtained from the dissociation hydrogen pressure in equilibrium with the hydride by expanding the liberated gas into preevacuated standard volumes.

3. Analytics. Gas analysis was carried out with a gas chromatograph HP 5890 employing a 5A molecular sieve and a Porapak Q column. In addition, an in-line mass spectrometer from Balzers type QMG 311 was used.

X-ray Debye–Scherrer diffraction patterns were obtained with a Siemens diffractometer U 13-007, using the Cu Kα radiation.

X-ray photoelectron spectra (XPS) and Auger electron spectra (AES) were determined with a VG ESCALAB 5 electron spectrometer (VG Scientific, East Grinstead, UK) described in detail elsewhere.[6] For the determination of XPS depth profiles the samples were degassed and pretreated inside the preparation chamber of the spectrometer by sputtering with an argon beam (15 μA/3 keV) emitted from a Penning ion source IQP 10/63, which was supplied by Leybold-Heraeus (Köln, FRG) and operated with a current density of about 20 nA mm^{-2}. For the AES depth profile investigations a scanning argon sputter gun (VG, AG 61; 5 keV, 25 nA mm^{-2}) was employed. A rough estimation for the conversion of sputtering times into corresponding depths was obtained by using average ion-induced sputtering yields of the pure metals.[7]

Scanning electron microscopy was carried out with a Type SR50A microscope from ISI (Japan) and energy-dispersive X-ray

(1) Willin, E.; Sirch, M.; Penzhorn, R.-D.; Devillers, M. *Fusion Technol.* **1988**, *14*, 756.
(2) Konishi, S.; Inoue, M.; Yoshida, H.; Naruse, J.; Sato, H.; Muta, K.; Inamura, Y. *Fusion Technol.* **1988**, *14*, 596.
(3) Penzhorn, R.-D.; Devillers, M.; Sirch, M. *J. Nucl. Mater.* **1990**, *170*, 217.
(4) Padurets, L. N.; Chertkov, A. A.; Mikheeva, V. I. *Russ. J. Inorg. Chem.* **1977**, *22*, 1750.
(5) Boffito, C., personal communication.
(6) Moers, H.; Pfennig, G.; Klewe-Nebenius, H.; Penzhorn, R.-D.; Sirch, M.; Willin, E. *KfK-Bericht 4449*, Sept, 1988.
(7) Matsunami, N.; Yamamura, Y.; Itikawa, Y.; Itoh, N.; Kazumata, Y.; Miyagawa, S.; Morita, K.; Shimizu, R.; Tawara, H. *At. Data Nucl. Data Tables* **1984**, *31*, 1.

0897-4756/90/2802-0255$02.50/0

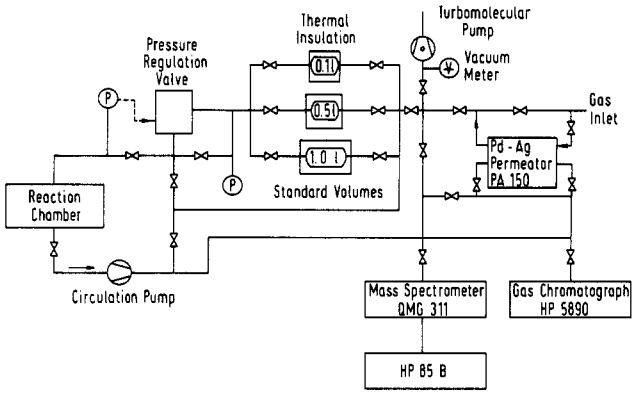

Figure 1. Scheme of the apparatus used for hydrogen/intermetallic compound volumetric loading/deloading studies.

Table I. Microprobe Analysis: Surface Distribution of Zr and Co on the ZrCo Alloy

surface type[a]	Zr density[b]	Co density[b]	Zr/Co
I	1914	1133	1.72
II	1177	1030	1.14

[a] See text for meaning of type I and II. [b] Arbitrary units.

analysis with a Kevex X-ray 7000 Instrument, Model 3201-600-V.

Thermal analysis was performed with a Netzsch Analyzer STA 409 (Selb, FRG) under an argon atmosphere.

BET specific surface areas of the employed materials were measured with an areameter manufactured by Ströhlein (Kaarst, FRG) using nitrogen.

Results and Discussion

1. Characterization of the ZrCo Ingot. 1.1. Microprobe Analysis. The topographic features of the surfaces were observed by scanning an electron beam across the surface of the sample and detecting the secondary electrons (SEI picture). From an analysis of the simultaneously generated X-rays information was obtained on the surface distribution of the elements (see Table I).

Two different kinds of surfaces were examined: (i) the face in contact with the cooling crucible in which the molten alloy solidified (type I) and (ii) a face created by mechanical rupture of the ingot (type II). The X-ray fluorescence spectra show surface segregation with higher relative Zr abundance on the surface of type I (see Figure 2). This observation is in line with the results given in Table I, which indicate that the Zr/Co ratio is significantly lower in the bulk of the material. A slight iron contamination originating from the cooling mould was detected only on surface I.

1.2. XPS and AES Surface Analysis. XPS measurements performed on as-received ZrCo ingot showed significant Zr enrichment on the outer surface, in qualitative agreement with the microprobe findings. Depending on the various samples investigated, the Zr/Co ratio was found to vary within large limits but was systematically higher for surfaces of type I ($10 < Zr/Co < 100$, mean value = 30) than for surfaces of type II (Zr/Co = 4).

Qualitative information on the various species present on the surface of the material was provided by the XPS elemental spectra by using the following photopeaks: Zr $3d_{5/2}$, Co $2p_{3/2}$, O 1s, and C 1s. Cobalt was found to appear mainly as $Co(OH)_2$ (781.8 eV) and partly in the metallic form (778.7 eV) together with some oxidic species. The systematic presence of an overlaying phase of ZrO_2 was inferred from the Zr $3d_{5/2}$ electron binding energy (182.6 eV). Evidence was obtained for a contamination of all surfaces by oxygen, carbon, and sodium. In addition, some other minor impurities such as F, Fe, N, Cu, and Si were

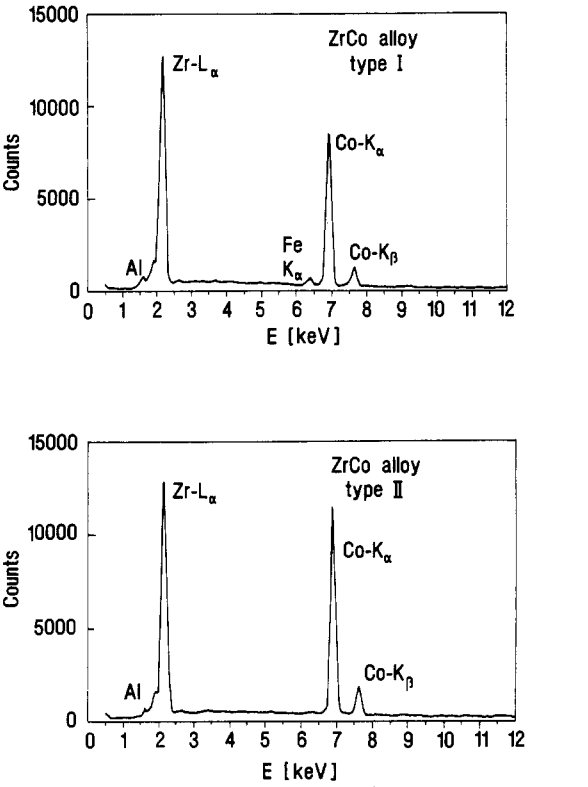

Figure 2. Microprobe analysis of type I and type II surfaces of ZrCo alloy (see text for meaning of type I and II).

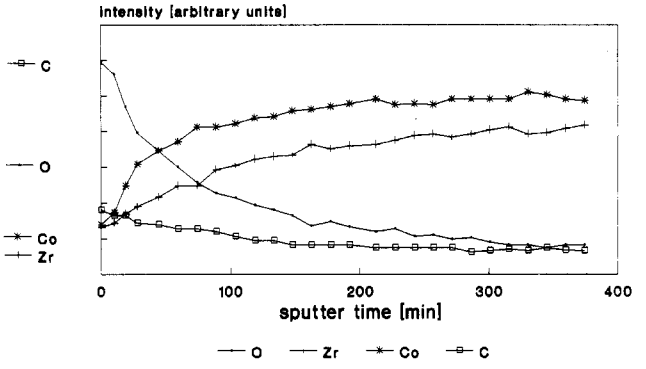

Figure 3. AES depth profile of type II surface of ZrCo alloy (see text for meaning of type II). The intensities correspond to the peak to peak heights of the differentiated Auger lines: Co, $L_4M_{45}M_{45}$; Zr, $M_4N_{23}N_{45}$. The intensities from the unsputtered surface are marked by the position of the symbols on the left-handed side. The total sputter time scale roughly corresponds to a depth of ca. 150 nm (it cannot be taken as linear due to the varying and unknown sputtering properties of the alloy surface).

detected on surfaces of type I. The carbon and oxygen intensities on type I and II surfaces decreased with progressive sputtering, the intensity of the oxygen peak reaching nonzero constant values at a depth of ca. 100 nm for both type I and type II surfaces.

The presence of ZrO_2 on the surface is common to all zirconium alloys[8-11] and is attributed to the very large negative free energy of formation of this compound. The cobalt depletion of the surface is usually explained by the

(8) Watanabe, E.; Ichimura, K.; Ashida, K.; Matsuyama, M.; Takeuchi, T. *Fusion Technol.* **1988**, *14*, 729.
(9) Ichimura, K.; Ashida, K.; Watanabe, K. *J. Vac. Sci. Technol.* **1985**, *A3*, 346.
(10) Wright, R. B.; Jolley, J. G.; Owens, M. S.; Cocke, D. L. *J. Vac. Sci. Technol.* **1987**, *A5*, 586.
(11) Wright, R. B.; Hankins, M. R.; Owens, M. S.; Cocke, D. L. *J. Vac. Sci. Technol.* **1987**, *A5*, 593.

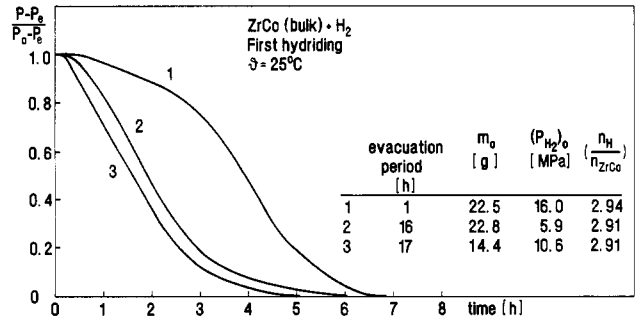

Figure 4. Effect of pretreatment on the induction period of the reaction of bulk ZrCo with hydrogen.

preferential oxidation of zirconium and diffusion of this element to the surface. The AES depth profiles support this explanation (see Figure 3). In general, type I and type II surfaces revealed similar depth profiles. Quantitative differences are probably due to different roughnesses and structures of both surface types.

When ZrCo alloy was heated under vacuum (10^{-6} Pa) at 500 °C for increasing periods of time, the material was found to behave very differently from the pure metal components. During the initial phase of the thermal treatment the Zr and O photopeaks were shifted to higher binding energies (+0.6 eV), indicating changes in Zr–O bonding; the cobalt and carbon photopeaks instead remained unchanged. The main variations in surface composition suggest desorption of the contaminating carbon layer, diffusion of oxygen into the bulk, and accelerated reduction of the Co^{II} species into Co^0, a process that takes place much more readily than in an air-oxidized Co sample. In contrast to the behavior of air-oxidized zircaloy-4 samples, where reduction of ZrO_2 to the metal occurs already at 300 °C through a suboxide state,[12] no reduction of ZrO_2 was observed with ZrCo upon heating up to 500 °C. Only after prolonged heating at the latter temperature a Zr $3d_{5/2}$ peak at a binding energy of 181.1 eV was observed, which according to previous investigations[13,14] can be assigned to nonstoichiometric oxidic species with lower oxidation stage, referred to as "zirconium suboxide". These observations could be explained by considering the oxygen solubility in the respective metals. While the high solubility of oxygen in zirconium favors the incorporation of this contaminant into the bulk and hence the generation of a metallic surface, this is not the case with cobalt, in which the oxygen solubility is known to be very low. When both metals are alloyed, the individual effects are probably less pronounced. This could account for the accelerated reduction of the cobalt oxide and the comparatively slow disappearance of ZrO_2. A more detailed report on the surface characterization of this material has been published elsewhere.[15]

From the above it is concluded that (i) the ZrCo alloy employed is of high purity, (ii) its composition is very closely given by ZrCo, and (iii) the reduction of zirconium oxide present on the surface of ZrCo proceeds much slower than on pure zirconium.

2. Activation of ZrCo Alloy. Large samples of ZrCo alloy powder in the hydride form were prepared by high pressure hydrogenation ($0.4 < p_{H_2} < 17.5$ MPa) of small pieces of the alloy ingot (each of about 10 g) at room temperature. The approximate hydrogen content of the samples was determined by weighing and by thermogravimetry. The mean loading from 14 different experiments with excess hydrogen was found to be $ZrCoH_x$ with $x = 2.91 \pm 0.04$, which yields a stoichiometry close to $ZrCoH_3$ (see Table II and ref 4).

Table II. High-Pressure Loading of Bulk ZrCo at Room Temperature

			BET specific surface area,[b] m^2/g	
P_{H_2},[a] MPa	m, g	$ZrCoH_x$ x	hydride	activated alloy
1.1	18.3	2.89 ± 0.02	0.53	
1.3	15.0	2.88 ± 0.02		
2.0	33.3	2.88 ± 0.01		
3.3	34.7	2.92 ± 0.01	0.64	0.45
5.7	29.1	2.92 ± 0.01	0.59	0.41
6.4	24.8	2.96 ± 0.01	0.57	0.43
6.5	25.1	2.96 ± 0.01	0.58	0.43
6.8	27.8	2.89 ± 0.01	0.73	0.37
8.0	12.7	2.85 ± 0.02		
8.6	30.3	2.96 ± 0.02		
9.8	12.2	2.89 ± 0.05		
9.8	14.4	2.91 ± 0.02	0.61	0.37
12.3	20.3	2.95 ± 0.01		
13.4	22.5	2.94 ± 0.01	0.52	0.39
	mean values	2.91 ± 0.04	0.60 ± 0.06	0.40 ± 0.03

[a] Excess H_2 pressure over the saturated hydride. [b] Obtained after dehydrogenation of the hydride first at 500 °C for 4 h and then at 700 °C for 1 h at 10^{-4} Pa.

As illustrated in Figure 4, the length of the evacuation period has significant influence on the induction period of the reaction of hydrogen with the ingot. While an induction period of about 30 min, followed by an initial slow reaction rate, is observed after pumping for about 1 h (see curve 1), after an evacuation of more than 15 h the reaction begins within a few minutes with a nearly constant rate (0.07 ± 0.02 mol of H_2 h^{-1}) up to a high degree of loading (curves 2 and 3). Saturation loading of the ZrCo ingot could also be attained within a few minutes, when the hydrogenation was carried out under heating in the temperature range 80–120 °C. In all runs a decrepitation of the ingot was observed, caused by the drastic change in density resulting from the incorporation of hydrogen atoms into the lattice. The corresponding volume expansion amounts to about 20%; the specific surface area of the obtained powder was found to be 0.60 ± 0.06 m^2/g (see Table II). This hydride powder could be handled under air without ignition.

To produce activated ZrCo powder, the hydride was dehydrogenated under high vacuum (10^{-4} Pa), first at 500 °C for 4 h and then at 700 °C for another hour. Under these conditions a material with a specific surface area of 0.40 ± 0.03 m^2/g was obtained (Table II). Dehydrogenation at temperatures above 700 °C yielded a sintered material with specific surface areas as low as 0.02 m^2/g.

The comparatively low reactivity of ZrCo ingot fragments toward hydrogen can be tentatively explained by two effects: (i) surface segregation with lower Co abundance associated to a reduced catalytic activity of Co for the adsorption of hydrogen; (ii) homogeneous coverage of the material by a ZrO_2 surface layer. Upon activation under a reducing H_2 atmosphere the ingot splits into nonsegregated high specific surface area granules and powder essentially not covered by ZrO_2.

3. Surface Characterization of the Hydride. Attempts to hydride ZrCo pieces inside the electron spectrometer were restricted by the maximum achievable hydrogen pressure (10^{-3} Pa). Under these conditions the

(12) Kaufmann, R. *KfK-Bericht 4417*, July 1988.
(13) Sen, P.; Sarma, D. D.; Budhani, R. C.; Chopra, K. L.; Rao, C. N. R. *J. Phys. F: Met. Phys.* **1984**, *14*, 565.
(14) de Gonzalez, C. O.; Garcia, E. A. *Surf. Sci.* **1988**, *193*, 305.
(15) Bredendiek-Kämper, S.; Klewe-Nebenius, H.; Pfennig, G.; Bruns, M.; Devillers, M.; Ache, H. J. *Fresenius Z. Anal. Chem.* **1989**, *335*, 669.

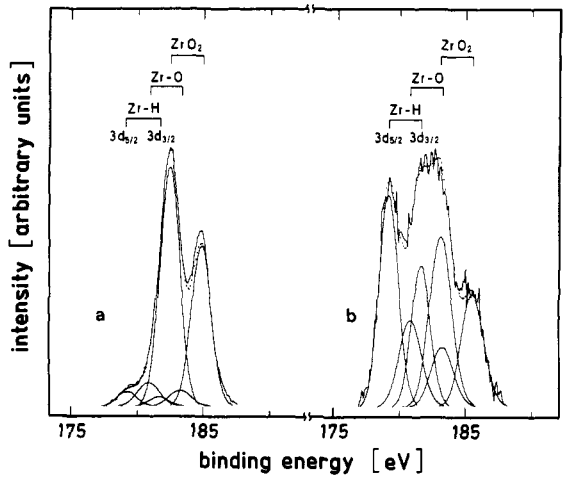

Figure 5. X-ray photoelectron spectra of the Zr 3d multiplet in $ZrCoH_{0.95}$ before (a) and after sputtering up to a depth of 30 nm (b).

depth profiles showed increased intensities of the metal peaks but no change in binding energies.

When a bulk ZrCo sample was exposed to 100 kPa of hydrogen at room temperature up to a loading of $ZrCoH_{0.95}$ to avoid pulverization and this sample was transferred into the electron spectrometer under an argon atmosphere, only the peaks characteristic of ZrO_2 and a C and O contamination were observed. The same peaks appeared with equal intensity after heating ZrCo for 2 h at 500 °C.

XPS measurements performed on the hydrogenated material before and after sputtering up to a depth of 30 nm are shown in parts a and b of Figure 5, respectively. In addition to the typical surface component signals (ZrO_2 and a Zr suboxide), another signal was detected at 179.6 eV, i.e., 0.4 eV higher than that of Zr^0 in ZrCo alloy. This value agrees well with that reported for Zr–H in $ZrCoH_3$[16,17] if the influence of the H_2 concentration on the binding energy of the Zr peak is taken into account.[18] The chemical shift of the Zr 3d level to higher binding energies indicates an electron transfer from the metal to the hydrogen atom. On the other hand, the hydridation was found to have no effect on the Co $2p_{3/2}$ binding energy, suggesting that upon hydriding the charge adjustments proceed only through electron density withdrawal from Zr atoms. Analogous observations have been reported for ZrNi.[16]

4. X-ray Investigations. The crystal lattice of the intermetallic ZrCo compound has a bcc structure with a_0 = 319.6 pm.[19] This phase could be contaminated by other phases such as the $ZrCo_2$ Laves phase, which forms solid solutions of the $MgCu_2$ type over the composition range 66–73 at % or 55–64 wt % Co, by the ZrCo + $ZrCo_2$ eutectic at the composition 53.4 at % or 42.5 wt % Co, or by the Zr_2Co tetragonal phase at the composition 33.3 at % or 24.4 wt % Co, all of them next to that of ZrCo in the phase diagram.[20–22]

(16) Nefedov, V. I.; Saln', Y. V.; Chertkov, A. A.; Padurets, L. N. *Russ. J. Inorg. Chem.* **1974**, *19*, 785.
(17) Gupta, M.; Schlapbach, L. Hydrogen in Intermetallic Compounds I. *Top. Appl. Phys.* **1988**, *63*, 179.
(18) Fujimori, A.; Schlapbach, L. *J. Phys. C.: Solid State Phys.* **1984**, *17*, 341.
(19) Pechin, W. H.; Williams, D. E.; Larsen, W. L. *ASM Trans. Q* **1964**, *57*, 465.
(20) Hossain, D.; Harris, I. R.; Barraclough, K. G. *J. Less Comm. Met.* **1974**, *37*, 35.
(21) Harris, I. R.; Hossain, D.; Barraclough, K. G. *Scr. Met.* **1970**, *4*, 305.
(22) Gachon, J. C.; Dirand, M.; Hertz, J. *J. Less Comm. Met.* **1982**, *85*, 1.

Table III. Pretreatment of Samples Characterized by X-ray Diffraction

sample	previous treatment	T_A,[a] °C	t,[b] h	cooling procedure[c,f]
1A	*d*	500	5	W
1B	*d*	900	72	W (5f)
1C	*d*	1100	3	W
1D	*d*	300	120	W
1E	*d*	400	120	W
2A	1A	500	24	W
2B	1A	500	120	W (5a)
3A	1C	1100	24	R (5d)
3B	1B	1100	120	R (5e)
4A	*e*	900	24	R (5b)
4B	*e*	900	24	S (5c)
4C	*e*	700	24	R

[a] Annealing temperature. [b] Annealing time. [c] See text for the meaning of the symbols W, R, and S. [d] Ten hydriding/dehydriding cycles with 100 kPa of H_2 at temperatures between 25 and 300 °C, deloading at 450 °C. [e] High-pressure loading (200 °C/10.5 MPa of H_2) followed by deloading for 4 h at T > 400 °C (T_{max} = 750 °C). [f] See Figure 6.

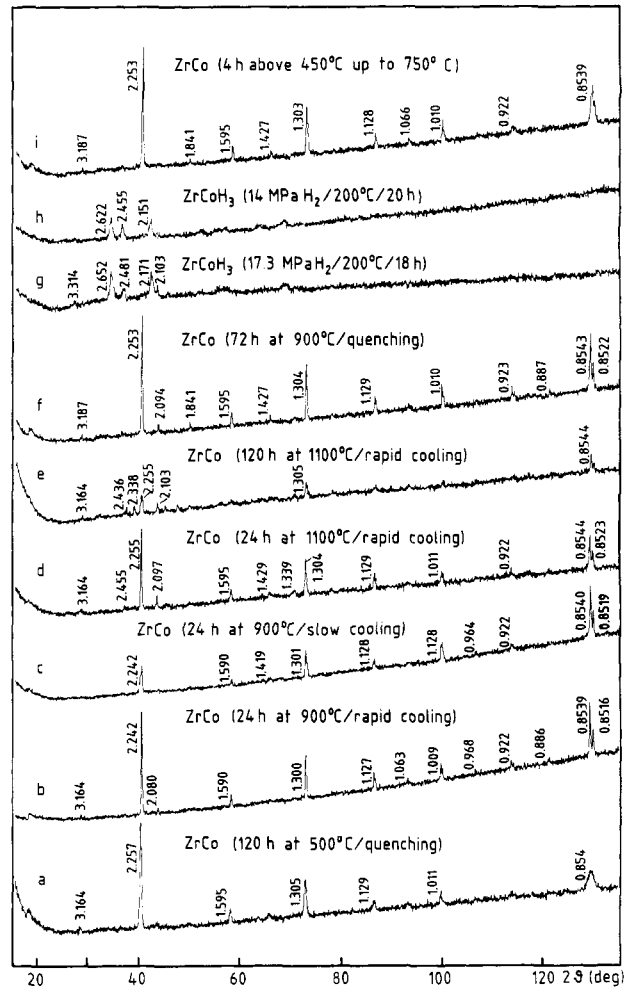

Figure 6. X-ray diffraction spectra of ZrCo (a–f, i) and $ZrCoH_3$ (g, h).

The appearance of the eutectic can be explained by the preferential oxidation of surface Zr atoms according to the reaction

$$3ZrCo + O_2 = ZrCo_2 + ZrCo + ZrO_2 \quad (1)$$

The segregation was observed by microprobe surface analysis, and the presence of ZrO_2 on the surface was confirmed by XPS and AES.

Untreated ZrCo specimens obtained by mechanical pulverization of small pieces of the original ingot showed poorly resolved diffraction patterns. To increase the degree of crystallinity, the powdered samples were annealed under a variety of conditions. After heating between 300 and 1100 °C in vacuum-sealed quartz tubes for periods between 3 h and 5 days, they were cooled either slowly inside the furnace (S) or rapidly outside the furnace (R) or else cooled by dropping the hot quartz tube into water (W) (see Table III and Figure 6).

The X-ray diffraction patterns of quenched ZrCo samples annealed at moderate temperatures (300–500 °C) exhibit the expected ZrCo lines; the lines show appreciable widths with poor resolution particularly at the high reflection angles, suggesting a low degree of crystallization (Figure 6a). Annealing experiments performed in the temperature region 700–1100 °C gave rise to samples showing narrow lines and a better resolution over the entire diffraction pattern, provided the samples were rapidly quenched down to room temperature (Figure 6b,f). Slow cooling after annealing at 900 °C for 1 day was found to modify the relative intensities of the major lines (Figure 6c). Heating ZrCo to temperatures above 900 °C followed by rapid cooling caused the appearance of small new lines, i.e., 2.080–2.097, 2.338–2.455, which were assigned to the $ZrCo_2$ Laves phase (Figure 6b,d). After prolonged heating of ZrCo at 1100 °C, most lines of the diffraction pattern disappeared (Figure 6e).

The hydrided samples showed a very poorly resolved X-ray diffraction pattern with only three broad lines appearing in the 2ϑ range 34–42° (Figure 6h). This result was found to be independent of the degree of crystallinity of the starting material (Figure 6g). The X-ray diffraction spectrum shown in Figure 6g was obtained after hydrogenation of the sample that gave rise to the X-ray spectrum shown in Figure 6f. Exposure of ZrCo powder to high pressures of hydrogen in the temperature range 25–200 °C did not improve the diffraction pattern. The obtained diffraction data were found to be in satisfactory agreement with values calculated for $ZrCoD_3$ from neutron diffraction experiments.[23]

The dehydrogenation of ZrCo hydride powder at 450 °C or above under a vacuum of 10^{-4} Pa yielded a finely divided powder, whose degree of crystallinity was found to depend upon the duration and temperature at which the dehydridation was carried out (Figure 6i). This indicates that it is possible to obtain a well-crystallized alloy at moderate temperatures (450 °C) and without quenching or rapid cooling.

5. H_2/D_2 Absorption/Desorption Isotherms. 5.1. Pressure–Composition Isotherms. Pressure–composition isotherms for the loading and deloading processes of the $ZrCo/H_2$ and $ZrCo/D_2$ systems were determined in the temperature range 150–300 °C by employing a volumetric procedure (Figure 7). Two different samples, one obtained from SAES, Italy, and the other from JAERI, Japan, were used in these experiments. The isotherms obtained with the two samples were practically identical. In agreement with previous data from Nagasaki et al.[24] and from Kost et al.,[25] the isotherms show slightly sloping plateaus at the higher temperatures within the composition range $ZrCoH_{0.5}$–$ZrCoH_{2.0}$, the length of the plateaus decreasing with increasing temperature. Neither the isotherms reported

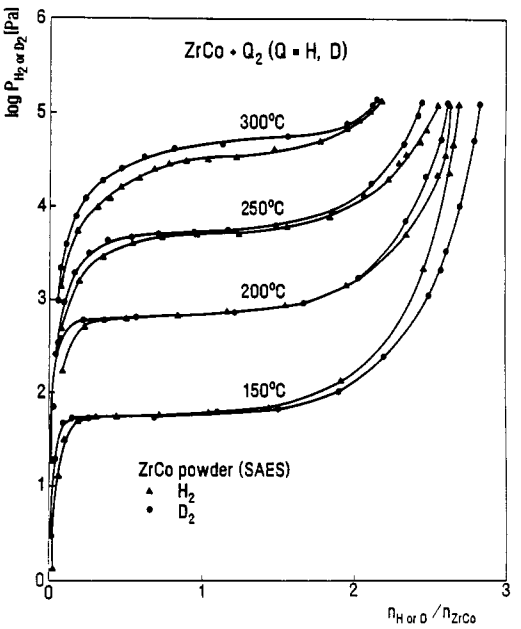

Figure 7. Pressure–composition isotherms for the $ZrCo/H_2$ and $ZrCo/D_2$ systems.

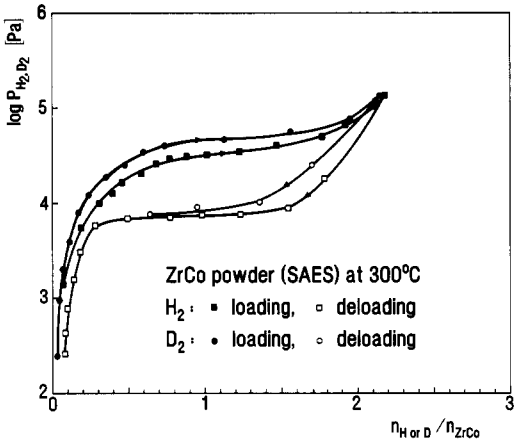

Figure 8. Hysteresis effect for the systems $ZrCo/H_2$ and $ZrCo/D_2$.

by Nagasaki et al. nor the ones obtained in this work show any evidence of the existence of two hydride phases such as reported by Irvine and Harris.[26]

In line with previous observations by Kost et al.,[25] the equilibrium pressures of D_2 over the ZrCo deuteride were found to be somewhat higher than those of H_2 over the corresponding hydride at temperatures above 250 °C.

5.2. Hysteresis Effect. Similar to many metal–hydrogen systems[27-29] the ZrCo–hydrogen system shows a pronounced systematic hysteresis effect, as apparent from a comparison between the absorption and desorption isotherms of H_2 and D_2 shown in Figure 8. For a given gas to metal ratio in the solid phase the desorption equilibrium pressure is significantly lower than the corresponding pressure in the absorption process.

From thermodynamic considerations and pressure–composition data, the hysteresis effect can be quantified by the so-called "hysteresis factor" f_h, defined as

$$f_h = RT/2 \ln P_a/P_b \quad (I)$$

(23) Irodova, A. V.; Somenkov, V. A.; Shil'shtein, S. Sh.; Padurets, L. N.; Chertkov, A. A. *Sov. Phys. Crystallogr.* **1978**, *23*, 591.
(24) Nagasaki, T.; Konishi, S.; Katsuta, M.; Naruse, Y. *Fusion Technol.* **1986**, *9*, 506.
(25) Kost, M. E.; Padurets, L. N.; Chertkov, A. A.; Mikheeva, V. I. *Russ. J. Inorg. Chem.* **1980**, *25*, 471.
(26) Irvine, S. J. C.; Harris, I. R. *J. Less Comm. Met.* **1980**, *74*, 33.
(27) Lundin, C. E.; Lynch, F. E. *Hydrides of Energy Storage*; Andresen, A. F., Maeland, A. J., Eds.; Pergamon Press: Oxford, England, 1978; p 395.
(28) Flanagan, T. B.; Clewley, J. D. *J. Less Comm. Met.* **1982**, *83*, 127.
(29) McKinnon, W. R. *J. Less Comm. Met.* **1983**, *91*, 293.

Table IV. Hysteresis "Factor" f_h (in kJ/mol of H or kJ/mol of D) at Various Temperatures and $ZrCoQ_x$ (Q = H or D) Compositions

	$f_h(H_2)$			$f_h(D_2)$
x	T = 200 °C	T = 250 °C	T = 300 °C	T = 300 °C
0.5	nd[a]	nd	2.14	nd
0.8	nd	nd	3.18	3.95
1.0	nd	nd	3.29	4.11
1.2	nd	nd	3.51	4.11
1.5	nd	3.30	3.67	3.12
1.8	nd	3.45	2.85	0.27
2.0	2.63	2.70	1.70	nd
2.2	1.72	1.80	nd	nd
2.4	1.04	0.75	nd	nd

[a] Not determined.

Table V. A and B Values According to Eq II for $ZrCoH_{0.8}$

sample	A	B	ref
JAERI	4751 ± 183	12.74 ± 0.35	this work
SAES	4266	11.80	this work
JAERI	3986	11.21	24
	4408[a]	12.04[a]	26

[a] Estimated from pressure–composition–temperature.

where P_a and P_d are the equilibrium pressures in the absorption and desorption process, respectively. The factor f_h actually represents the loss of Gibbs free energy per mol of H during a hydriding/dehydriding cycle. A few values of f_h calculated for the systems $ZrCo/H_2$ and $ZrCo/D_2$ have been compiled in Table IV. The mean values of f_h calculated for the $ZrCo/H_2$ and $ZrCo/D_2$ systems at 300 °C in the plateau region ($ZrCoH_x$ or $ZrCoD_x$ with $0.8 < x < 1.5$) are 3.41 ± 0.22 kJ/mol of H and 3.82 ± 0.47 kJ/mol of D, respectively.

5.3. Thermodynamics. For a given hydrogen/metal ratio, the temperature dependence of the equilibrium pressure can be described by the relationship

$$\log P_{H_2 \text{ or } D_2} = -A/T + B \qquad \text{(II)}$$

in which P is the pressure (pascals) and T the temperature (kelvin). At the composition $ZrCoH_{0.8}$ a comparison of A and B values obtained in this work with data given in or calculated from the literature is presented in Table V. The data show satisfactory agreement between the results obtained here for ZrCo samples of different origin and those published in the literature.

Numerous investigations have dealt with the equivalence of the empirical terms A and B of eq II and the thermodynamic functions ΔH and ΔS, which characterize the interaction of H_2 with a metal or an intermetallic compound.[30,31]

Pressure–composition isotherms can involve three successive processes:

(i) dissolution of hydrogen in the metal

$$M(s) + y/2H_2(g) = MH_y(s)\ (\alpha\text{-phase}) \qquad (2)$$

(ii) conversion of the saturated solid solution (α-phase) into a nonstoichiometric hydride (β-phase) under constant pressure

$$MH_y(s) + (x - y)/2H_2(g) = MH_x(s) \qquad (3)$$

(iii) further dissolution of hydrogen in the β-phase according to

$$MH_x(s) + (s - x)/2H_2(g) = MH_s(s) \qquad (4)$$

where MH_s represents the stoichiometrically saturated hydride.

When both the solubility of hydrogen in the α-phase and the deviation of the hydride composition from stoichiometry are negligible, i.e., $y \approx 0$ and $x \approx s$, the standard enthalpy of formation ΔH_f and the standard entropy of formation ΔS_f of the hydride can be estimated from the integrated van't Hoff equation:

$$\ln p_{H_2} = (2/sR)(\Delta H_f/T - \Delta S_f) \qquad \text{(III)}$$

where

$$K_P = p_{H_2}^{-s/2} \quad (p \text{ in bar}) \qquad \text{(IV)}$$

and p_{H_2} denotes the hydrogen equilibrium dissociation pressure in the plateau region. It is assumed that ΔH_f is constant over the contemplated temperature range.

When the conditions mentioned above are not rigorously fulfilled, the thermodynamic data obtained from a log P vs $1/T$ plot in the plateau region cannot be assigned to the formation of the stoichiometric hydride. In practice, however, it is often assigned to the reaction taking place in that region, i.e., the α–β conversion. An additional constraint is that both the solubility and the deviation from stoichiometry are temperature dependent. Despite these limitations, the approach discussed above is considered useful for an estimation of the thermodynamic parameters of a metal/hydrogen or an intermetallic/hydrogen system. In fact, satisfactory agreement is usually observed between ΔH_f values calculated from pressure–composition–temperature data and those obtained directly from calorimetric experiments.

In the case of the $ZrCo/H_2$ system several particularities need to be taken into account: the solid solution region is rather extensive, the plateaus are slightly sloping, and both extent and slope of the plateaus are strongly temperature dependent.

With the pressure–composition–temperature data of this work, values for the apparent molar enthalpy and entropy of hydrogen absorption were calculated for the process taking place in the plateau region, i.e.

$$ZrCoQ_y + (x - y)/2Q_2 = ZrCoQ_x \quad (Q = H \text{ or } D) \qquad (5)$$

where $ZrCoQ_y$ and $ZrCoQ_x$ represents the saturated α-phase and the nonstoichiometric hydride (or deuteride), respectively. Combining eq II–IV, one obtains

$$\log P_{Q_2} = -A/T + B = \Delta H_{Q_2}/2.3RT - \Delta S_{Q_2}/2.3R + 5 \qquad \text{(V)}$$

where P is in pascals and ΔH_{Q_2} and ΔS_{Q_2} are the enthalpy and entropy changes, respectively, occurring when 1 mol of Q_2 (H_2 or D_2) is absorbed by ZrCo, the standard state being defined at P = 100 kPa.

Table VI gives A and B parameters together with ΔH_{Q_2} and ΔS_{Q_2} values obtained from pressure–temperature data at various $ZrCoQ_x$ (x = H or D). The mean ΔH_{Q_2} and ΔS_{Q_2} values corresponding to the plateau region ($0.8 \leq x \leq 2.0$) agree very well with the enthalpy of formation of the hydride derived by Shilov et al.[32] from DTA experiments (ΔH_{H_2} = −83.3 kJ/mol). The agreement with the results of Irvine et al.[23] (ΔH_{H_2} = −84 kJ/mol, ΔS_{H_2} = −135 J/K·mol) and of Kost et al.[25] (ΔH_{D_2} = −99 kJ/mol) is satisfactory. The difference between the ΔS values for H_2 and D_2 absorption, e.g., 13.7 J/K·mol is essentially the same

(30) Flanagan, T. B. *Hydrides for Energy Storage*; Andresen, A F., Maeland A. J., Eds.; Pergamon Press: Oxford, England, 1978; p 42.
(31) Rudman, P. S. *Int. J. Hydrogen Energy* **1978**, *3*, 431.
(32) Shilov, A. L.; Padurets, L. N.; Kost, M. E. *Russ. J. Phys. Chem.* **1983**, *57*, 338.

Table VI. Van't Hoff Parameters and Thermodynamic Functions for the Absorption of H_2 and D_2 by ZrCo Alloy in the Plateau Region ($0.8 < x < 2.0$)

x	A	B	$-\Delta H$, kJ/mol	$-\Delta S$, J/mol·K
		Hydrogen		
0.8	4266	11.80	81.7	130.2
1.0	4311	11.91	82.5	132.3
1.2	4315	11.94	82.6	132.9
1.5	4346	12.06	83.2	135.2
1.8	4113	11.76	78.7	129.4
2.0	4216	12.12	80.7	136.3
mean values	4261 ± 85	11.93 ± 0.14	81.5 ± 1.6	132.7 ± 2.7
		Deuterium		
0.8	4537	12.46	86.9	142.8
1.0	4575	12.56	87.6	144.7
1.2	4604	12.64	88.1	146.3
1.5	4623	12.73	88.5	148.0
1.8	4579	12.73	87.7	148.0
2.0	4508	12.76	86.3	148.6
mean values	4571 ± 42	12.65 ± 0.12	87.5 ± 0.8	146.4 ± 2.3

as the standard entropy difference between gaseous deuterium and hydrogen, e.g., $S°_{D_2}(g) - S°_{H_2}(g) = 14.3$ J/K·mol, suggesting that the entropy difference between the solid deuteride and the solid hydride is very small.

At low temperatures the ZrCo deuteride is expected to be more stable than the corresponding hydride, i.e., the deuteride has a lower equilibrium pressure than the hydride. With the A and B values estimated over the plateau regions, dissociation pressures at room temperature of 4×10^{-3} and of 2×10^{-3} Pa were calculated for the hydride and the deuteride, respectively. Because of the dominance of the entropy term at higher temperatures, a reversal in stability is observed. With the data in Table VI, the temperature at which the stability crossover takes place is estimated to be 160 °C. A desorption equilibrium pressure of 100 kPa is reached at 342 °C with the hydride and at 325 °C with the deuteride, in line with the above-discussed stability considerations. It is concluded that the temperature required for the recovery of tritium from ZrCo tritide at a desorption pressure of 100 kPa is comparatively moderate. Corresponding experiments with tritium are in progress.

6. Isopleth Experiments. A few experiments were carried out at constant volume and constant ZrCo/hydrogen overall composition (isopleths), varying only the temperature. Some typical runs, presented in Figure 9, are compared with absorption/desorption isotherms at temperatures in the range 200–300 °C. Points 1 and 2, which were obtained in the isothermal absorption mode, fit well onto the reference absorption isotherm at 300 °C. Cooling to 151 °C (point 3) and heating again to 300 °C at constant overall composition ($n_{H_2}/n_{ZrCo} = 0.22$) gives rise to pressure–composition–temperature data defined by point 4, which lies just below the reference curve. The equilibrium pressure at 300 °C, which is established after further addition of hydrogen up to the composition $n_{H_2}/n_{ZrCo} = 0.67$, was also found to be consistent with the reference curve (point 5). Cycling the temperature again from 300 °C down to room temperature and up to 300 °C yielded an equilibrium pressure, which is significantly lower than the starting value and is located between the absorption and desorption isotherms at 300 °C (point 6). Cooling stepwise to 152 °C (point 7) and to room temperature and then reheating the hydride first to 152 °C (point 8) and then to 300 °C (point 9) gave rise to equilibrium pressures that agreed well with the original values, an indication of good reproducibility. The same type of behavior was observed when the temperature was cycled

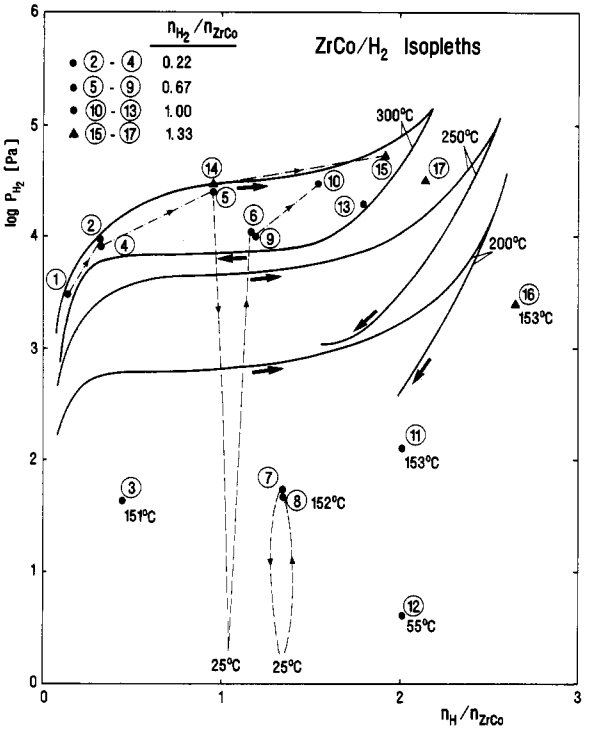

Figure 9. Comparison of $ZrCo/H_2$ isopleth data with $ZrCo/H_2$ absorption/desorption isotherms.

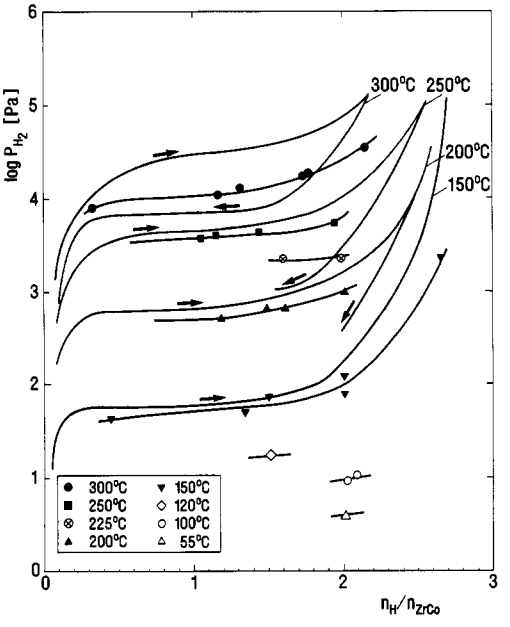

Figure 10. Comparison of isopleth and isothermal absorption/desorption for the system $ZrCo/H_2$.

after the addition of hydrogen up to $n_{H_2}/n_{ZrCo} = 1.0$ (points 10–13).

After the completion of the isopleth experiments discussed above the sample was heated to 450 °C, evacuated, and loaded again with hydrogen, first to $n_{H_2}/n_{ZrCo} = 0.96$ (point 14) and then to 1.92 (point 15). It is seen that the previous history of the sample has no influence on the absorption isotherm data. Upon further thermal cycling (300/153 °C), the characteristic behavior is again observed (points 15–17). Analogous observations studied only in the cooling mode have been reported for other intermetallic compounds.[33]

(33) Dantzer, P. *J. Less Comm. Met.* **1987**, *131*, 349.

Table VII. Isopleth Experiments[a]

data point[b]	$(n_{H_2}/n_{ZrCo})_{total}$	$(n_H/n_{ZrCo})_{hydride}$	% hydrogen		intermediate temp, °C
			gas phase	hydride	
2	0.22	0.32	28	72	150
4	0.22	0.33	25	75	
5	0.67	0.96	28	72	25
6	0.67	1.18	12	88	
10	1.00	1.55	23	77	150/55
13	1.00	1.74	14	86	
15	1.34	1.92	28	72	150
17	1.34	2.16	19	81	

[a] The temperature was cycled from 300 °C down to various intermediate temperatures and back to 300 °C employing n_{ZrCo} = 0.0364 mol. [b] See Figure 9.

Table VIII. Van't Hoff Parameters Calculated from Isopleth Data within the Plateau Region at Temperatures in the Range 150–300 °C According to

$$\log p = -A/T + B^a \quad \text{(II)}$$

n_H/n_{ZrCo}	A	B
0.8	3839	10.80
1.0	3844	10.83
1.2	3861	10.89
1.5	3829	10.93
1.8	3913	11.17
2.0	3940	11.33
mean value	3871 ± 45	10.99 ● 0.21

[a] p in pascals and T in kelvin.

In summary, the equilibrium pressures attained after cycling the temperature at constant overall composition within the plateau region are systematically somewhat lower than those of the absorption isotherms. The isopleth equilibrium pressures are reproducible and not due to a departure from equilibrium. This is substantiated by experiments showing that after about 15 min following a disturbance equilibrium is reattained and is not further changed even if the equilibration period is prolonged for 16 h. It is therefore concluded that temperature variations under isopleth conditions are associated with some hydrogen trapping in ZrCo, resulting in hydrogen pressures somewhat lower than the equilibrium absorption pressure. In an attempt to quantify this effect, the amount of hydrogen trapped at 300 °C in ZrCo after various heating cycles was calculated from the data in Figure 9 and listed in Table VII. From the results it is apparent that the trapping is essentially restricted to concentrations within the plateau region, i.e., $n_{H_2}/n_{ZrCo} > 0.4$.

A comparison between isopleth data and absorption/desorption curves obtained under isothermal conditions is given in Figure 10. The isopleth "isotherms" were obtained by joining data points corresponding to several constant H_2/ZrCo overall compositions. The departure of the isopleth curves from the absorption curves becomes notorious at 300 °C. Van't Hoff parameters in the plateau region for the isopleths are listed in Table VIII. With the mean A and B values calculated for the "isopleth plateau region" a room-temperature hydrogen equilibrium pressure of 10^{-2} Pa is calculated, and the temperature at which a dissociation pressure of 100 kPa is reached is estimated to be 375 °C.

Acknowledgment. We gratefully acknowledge the X-ray analysis carried out by U. Berndt, the BET measurements by H. E. Noppel, the assistance in the surface analytics by G. Pfennig, and the microprobe analysis by H. Clauss. We also thank S. Huber and H. R. Ihle for many valuable comments. M.D. expresses his gratitude for a fellowship from the European Communities (Fusion Technology Program). This work has been performed within the frame of the Nuclear Fusion Project of the Kernforschungszentrum Karlsruhe. It is supported by the European Communities within the European Fusion Technology Program.

Registry No. T_2, 10028-17-8; ZrCO (alloy), 77592-21-3; H_2, 1333-74-0; D_2, 7782-39-0.